Comparison between finite element and experimental evidences of innovative W lattice materials for sacrificial limiter applications

R. De Luca*[a], P. Fanelli[a], C. B. Hünteler[b], F. Vivio[c], K. Zhang[b], A. von Müller[b], G. Calabrò[a], F. Maviglia[d] and J. H. You[b]

[a]*University of Tuscia, DEIm Department, Via del Paradiso 47, 01100 Viterbo, Italy*
[b]*Max Planck Institute for Plasma Physics, Boltzmann Str. 2, 85748 Garching, Germany*
[c]*University di Rome "Tor Vergata", Enterprise Engineering Department, Via del Politecnico 1, 00133, Rome, Italy*
[d]*EUROfusion Consortium, PPPT Department, Garching, Boltzmannstr. 2, Germany*

Power exhaust is a key mission for the realization of fusion electricity. Engineering challenges may arise from the extreme heat fluxes developed during plasma transients, above the limit offered by existing materials. These can reduce the lifetime of plasma-facing components (PFCs), imposing extraordinary maintenance, reactor safety issues and ultimately delayed return to normal operation. Concerning the EU DEMO reactor, discrete sacrificial limiters are being investigated as the last safety resource of the reactor's wall in case of unmitigated events. Within this context, micro-engineered tungsten (W) lattices are proposed to cope with unmitigated plasma disruptions. Unlike bulk W, lattices can be tailored to meet the operational requirements of the limiter, compromise between steady-state and off-design performances while avoiding overloading of the heat sink and delay the need for extraordinary maintenance. By calibrating an equivalent solid model originally developed and validated for open-cell aluminum (Al) foams, tailored lattices have been modelled and samples fabricated through additive manufacturing for characterization and testing, currently ongoing.

In the present work, the thermal response of lattice samples during thermal shock high heat flux (HHF) tests performed at the linear facility QSPA Kh-50 facility is simulated using ANSYS and compared with available results. Enthalpy changes of W were imposed to simulate phase change. Good agreement with experiments and SDC-IC reference up to melting point was observed. Ultimately, a thermal quench of an unmitigated DEMO disruption was simulated involving an original MAPDL routine that removes mesh elements at the melting or vaporization point.

Keywords: DEMO, limiter, disruption, lattice, QSPA-Kh50, FEA, enthalpy, phase change

1. Introduction

Controlling the heat and particle exhaust inside a tokamak is a key issue towards the realization of nuclear fusion [1]. Inside a tokamak, the lifetime of plasma facing components (PFCs) is influenced by the harsh operating conditions they cope with, in terms of high heat flux, erosion, sputtering as well as additional limitations due to the presence of a neutron flux [2]. Currently, W is the preferred armor material owing to its high melting point, acceptable thermal conductivity, high sputtering threshold and low fuel retention. On the other hand, it is brittle at room temperature and a mismatch exists between its thermal expansion coefficient and that of heat sink materials. In present-day layouts of actively cooled PFCs, the heat sink is a structural part where the coolant flows to exhaust the heat. For this porpose, copper alloy (CuCrZr) and reduced activation ferritic-martensitic steels are to date the reference materials for actively cooled heat sink. Additionally, established manufacturing routes of W represent a limit to the design of advanced layouts [3]. Considering EU DEMO and future reactors, recent studies suggest that the greatest challenges of PFCs may arise from the occurrence of plasma transients, such as disruptions [4]. For instance, during unmitigated disruption thermal quench (TQ) the first wall (FW) will be exposed to wall power density in the order of tens of GW/m^2 for few ms [4]. The expected damage factor will be far greater than $50MJ/s^{0.5}m^2$ which is the limit of W [5]. Consequently, no existing material would be able to survive such an extreme amount of energy deposited. Surface vaporization, melting and re-solidification is therefore expected. In severe cases, an eventual failure of conventional PFCs might compromise the reactor safety and delays its return to normal operation. Furthermore, the design of DEMO FW components is currently based on the normal operation, when the heat loads are anticipated to be always below $1.5MW/m^2$ [6]. Disruptions should be avoided as much as possible in DEMO. An active field of research aims at developing predictive codes to promptly recognise the precursor of MHD instabilities that may trigger disruptions [7]. When controlled discharge shutdown is not possible, shuttered pellet and massive gas injection are employed as mitigation stratedy to reduce impact on the first wall components at the contact point. However, in the EU DEMO, this could still be not enough, and wall protection strategies are mandatory. These would represent the last resource to prevent the FW from excessive degradation.

Combined with mitigation and prevention strategies, sacrificial limiters are being proposed for the EU DEMO to prevent the direct interaction between the plasma and unshadowed wall [8]. In this context, the aim of this work is to develop a sacrificial limiter to cope with unmitigated upward disruptions. For this purpose, the sacrificial limier will be provided with newly-engineered lattices tailored to match its functional and conflicting requirements. In fact, on one hand adequate heat exhaust capability are needed to withstand the steady-state load in normal

*Corresponding author: dlriccardo @unitus.it

operation. On the other hand, when the disruption occurs, vapor shielding formation must be promoted and overloading of the heat sink must be avoided. In this regard, TOKES code predictions have provided encouraging results, with the wall heat flux significantly reduced (up to 8-10 times) when vapor shielding is involved [9]. By interposing a thermal insulator between the heat sink and the sacrificial armor, we might fulfil this goal. However, one can observe that normal and transient design requirements are conflicting with each other. In a previous study [10], we observed that unlike dense W, tailored open-cell lattices can be regarded as a promising sacrificial material: a proper design of their cell and ligaments can be carried out to tailor their thermo-mechanical response. By doing so, they could offer enhanced vapour shielding and perfect insulation of the heat sink against overloading. Moreover the larger design flexibility with respect to bulk W also helps achieve the needed trade-off between normal operation and transient requirements. Pioneeristic literature on W-based micro-engineered armors suggest foams and lattice structures as promising armor materials for transient applications in fusion [11]. Above all, ther peculiar rotation and deformation of ligaments results in less pronounced thermal stresses at high temperatures and more ductile behavior [12]. On the other hand, their geometrical features are hard to reproduce using conventional manufacturing routes of W. Additive manufacturing techniques have been employed to gain the design freedom for the fabrication of complex parts. In fact, recent studies have qualified Laser Powder Bed Fusion (LPBF) for the fabrication of complex W parts for fusion applications [13].

Recently, an existing solid model originally developed for Al open-cell foams [14] was calibrated to design optimized lattice geometries having 49.6% and 53.3% relative density but relative thermal conductivity respectively of 39.9% and 25.2% with respect to the base material. As part of the collaboration established between Tuscia and "Tor Vergata" University in the workframe of the EUROfusion WPDIV activity, W lattice samples have been successfully designed and fabricated by means of LPBF [15]. Material characterization is currently ongoing as well as thermal shocks high heat flux (HHF) testing on linear plasma devices, such as at the QSPA-Kh50 facility.

In the present work, preliminary evidences from the experimental campaign at QSPA Kh-50 [16] are compared with results from finite element (FE) analyses carried out in ANSYS. Enthalpy changes of W as well as an original MAPDL routine that removes the mesh elements at the melting or vaporization point were implementd to simulate phase change. Ultimately, the thermal quench of an unmitigated DEMO disruption thermal quench (TQ) was simulated. Conservative assumptions were imposed to the loads reported in [6]. After an initial stationary operation under 1.5MW/m^2, TQ was imposed consisting of 5GW/m^2 deposited in 2ms.

2. Cell geometry and optimized mesh

As shown in Fig.1, two sample layouts, called A and B model, were tested on QSPA Kh-50 [16]. Each sample is a 10x10x10 mm^3 cube obtained from the linear repetition of the regular elementary cell. The geometrical features of each cell variant are listed in Table 1 together with the correponsing relative density and relative thermal conductivity. *A* refers to the cell anisotropy, an index corresponding to the ratio between vertical and horizontal cell dimensions. *L* is the ligament length and r the radius of its cross section, both in mm. *f*, also included in the name of the sample, is the scaling factor with respect to the original model size. These two candidates were designed on the base of a parametric design optimization [10] targeting a combination of relative density $\bar{\rho} \approx 50\%$ and equivalent thermal conductivity along the building direction $\bar{\lambda} < 50\%$

Table 1. Characteristics of the two elementary cell variants

	A	L (mm)	r (mm)	f	$\bar{\rho}$ (%)	$\bar{\lambda}$ (%)	No. mesh elem
A167	1.6	0.33	0.15	1.67	49.6	39.9	124k
B278	0.5	0.57	0.25	2.78	53.1	25.2	144k

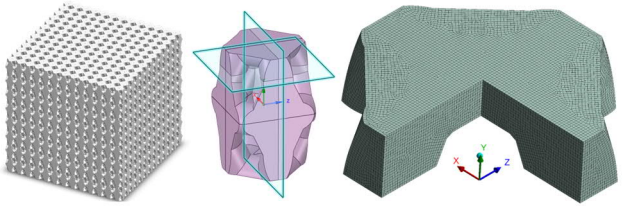

Figure 1: Geometries and optimized mesh of A167 sample

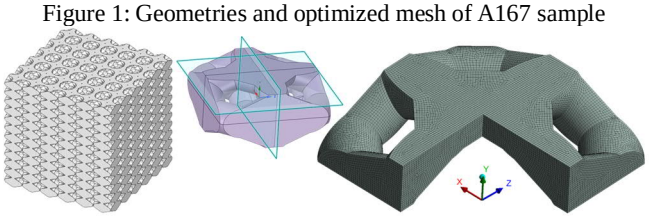

Figure 2: Geometries and optimized mesh of B278 sample

Figure 1 and Figure 2 report the cell geometries and the optimized meshes used in the ANSYS Workbench and Mechanical APDL 19.2 environment. After a convergence test, optimized meshes with less than 145k 20-node-hex. elements were obtained. In the context of this work, the mesh quality turned out to play a key role: since the transient duration is very short and non-linear material properties imposed, poor mesh quality led to anomalous hot spots and overestimated temperatures.

3. Modelling phase change

Aiming at reproducing the degradation of lattices during severe plasma transients in the EU DEMO, melting and vaporization of W were included in the simulation through enthalpy changes. We did not account for erosion, vapour shielding and melt motion since the major goal of the work was centered on the possibility to model the physics of vaporization and melting in finite element analysis. Enthalpy was defined in J/m^3, as a non-linear function of temperature valid from room temperature to vaporization, according to the following expression derived from thermodynamic principles:

$$\Delta H(T) \begin{cases} \int_{T_0}^{T} \rho(T)c_p(T)dT\,; & T \le T_{melt} \\ \Delta H_s + \Delta H_{melt} + \int_{T_{melt}}^{T} \rho(T)c_p(T)dT\,; & T_{melt} < T \le T_{vap} \\ \Delta H_s + \Delta H_{melt} + \Delta H_m + \Delta H_{vap}; & T > T_{vap} \end{cases}$$

The heat capacity, namely the product of density and specific heat $\rho(T)c_p(T)$, is the function to be integrated in temperature to obtain the sensible heat. According to this, ΔH_s flags the sensible heat corresponding to the integral solved between room temperature to melting (3422°C [17]) and with ΔH_m from melting to vaporization (5727°C [17]). ΔH_{melt} and ΔH_{vap} represent the latent heat respectively at melting and vaporization temperature. Ideally, this heat is a step variation for pure elements. However, convergence constrains imposed to spread it over a narrow temperature window, in the order of tens of °C. In recent literature [17], thermo-physical properties of W are provided as polynomial functions of temperature from room temperature to vaporization. From the same reference we derived the latent heat of melting ΔH_{melt}. Instead, the variation associated to vaporization was indirectly derived from the total sublimation enthalpy ΔH_{sub} suggested in [18]. From the enthalpy plot shown in Figure 3, one can appreciate that latent heat plays a significant role, being in sum 70% of the total sublimation energy, with near 90% of it provided by vaporization. Consequently, we speculate that this would be a beneficial feature for a sacrificial limiter to reduce the energy otherwise delivered to the solid wall.

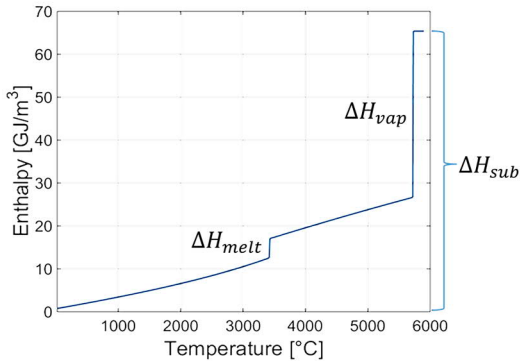

Figure 3: Enthalpy plot for modelling phase change of W

4. FE simulation of pulses at QSPA-Kh50 – Model Validation

QSPA-Kh50 is a linear plasma gun hosted at the KIPT Institute of Karchov, Ukraine. It is able to deliver up to 30MJ/m^2 plasma stream energy in 0.25ms, with initial target preheating up to 500°C [19]. Despite the very short pulse duration, plasma energy is compatible with the TQ in EU DEMO. Both plasma stream energy density Q and target (absorbed) energy density q are measured by calorimetry: the plasma stream energy by a movable calorimeters that can be protruded beyond the target whereas the absorbed energy is measured by small thermocouple calorimeters inserted into surface layers of the target. Previous tests performed on bulk W samples have revealed surface melting starting from $q = 0.6$MJ/m^2 and vaporization threshold around $q = 1.1$MJ/m^2 [20]. Above this, any further increase of Q does not affect q, which remains stable around 1.1MJ/m^2, most likely because of vapour shielding [20]. In Figure 4, preliminary results on model A167 lattice samples are marked in red. Two groups of 4 samples were exposed with energy of incoming plasma stream Q of 1.1MJ/m^2 (5 plasma pulses) and 1.8MJ/m^2 (5 plasma pulses) [16]. The initial temperature was set to 500°C and the measured target energy q was respectively 0.6MJ/m^2 and 0.85MJ/m^2. They showed a similar behavior to bulk W, but this is most likely due to the short pulse duration, which doesn't produce sufficient heat penetration in the lattice to reach the open porosity. This penetration depends on thermal diffusivity α and pulse duration t, being $\partial = \sqrt{\pi\alpha(T)t}$, as derived from the analytical solution of the Fourier equation for a semi-infinite medium [21]. The minimum penetration from the lattice's top to reach the porosity is in the order of 400µm, while in 0.25ms the penetration in bulk W is only 100µm.

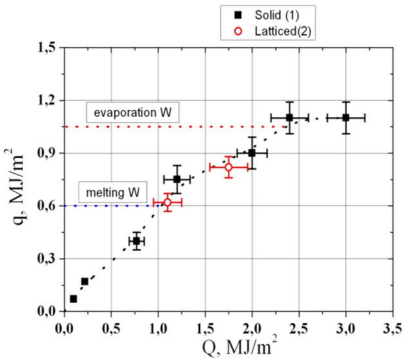

Figure 4: Preliminary results from QSPA-Kh50 performed on bulk and lattice samples, from [16]

Experimental evidences from QSPA-Kh50 were compared with the simulated thermal response of lattice samples after a single pulse, where the deposited energy is the same absorbed by the target. In quasi-optical approximation, being ion gyro radius of ions in QSPA quite larger than the dimensions of the open pores of the lattice, we assumed that the heat load remains shallow and mostly deposited to the top plasma-facing surface. Results reported in Figure 5 were obtained with the "non-linear" enthalpy of W and also repeated with the W reference properties from ITER SDC-IC reference. Globally, "non-linear" W was found capable of replicating the experiments with good similarity. At the lowest energy density the maximum temperature is around 3000°C. Incipient melting was expected, and indeed it is not far from being reached. However, by repeating the simulation with SDC-IC W properties almost identical results were obtained, confirming at least perfect agreement with the reference up to melting point. At the highest target energy, surface melting observed during experiments was also confirmed in simulations, with maximum temperatures of lattice samples up to 3960°C. Only small differences are observed by comparing results from bulk W, A and B geometries. Again, this suggests that the pulse duration in QSPA-Kh50 is too short for appreciating differences due

to the lattice geometry. In fact, from the temperature destributions in Figure 5 one can see that the thermal gradients are really shallow and do not propagate much within the 0.25ms of exposure time. Therefore, additional tests on devices able to sustain longer pulses will be pursued.

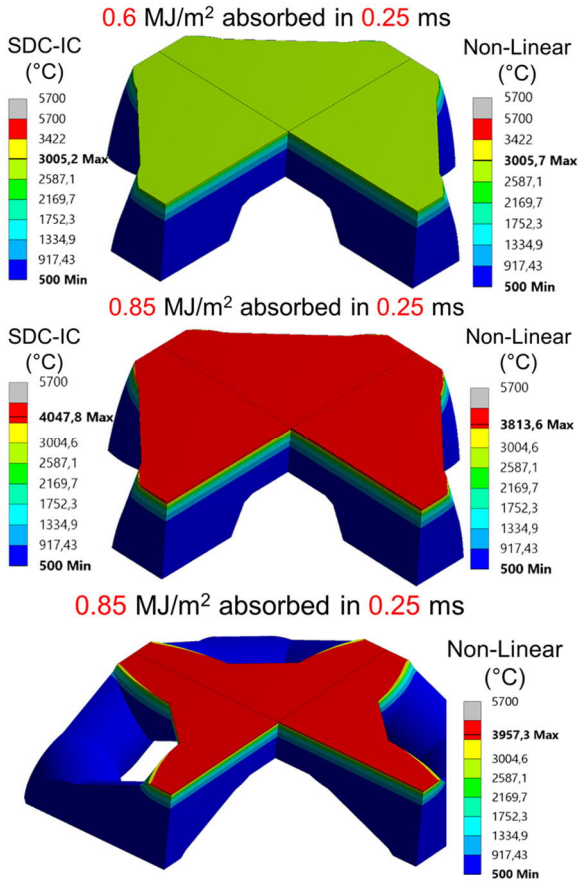

Figure 5: Simulated conditions during experiments at QSPA-Kh50. The first two cases refer to A model, and confirm similarity with experiments and tight agreement between non-linear W and reference material from SDC-IC. Third case is temperature distribution for the B model, found in the same range of those of A model.

5. EU DEMO scenario simulation

The thermal behavior of W lattices as sacrificial armor material for the PFCs of the EU DEMO upper limiter (UL) was assessed in ANSYS under preliminary assumptions. The considered layout of the PFC is based on the flat tile configuration in Figure 6 and is the result of a previous design optimization [10]. It consists of a water cooled heat sink in CuCrZr, provided with a 10mm thick armour consisting of W lattices (B278 layout), for a global size of 23x26.5mm. Even if a rectangular cooling channel is a viable option, a circular cooling channel with a diameter of 12mm was preliminarily chosen for analogy with alternative layouts based on the W monoblock [22]. Thermo-hydraulic water parameters (8m/s, 300°C, 15MPa, no swirl tape) were assumed as suggested in [8]. The heat transfer coefficient (htc) at the cooling pipe was applied as a function of the wall temperature, using the semi-empirical laws developed for actively cooled PFCs in nuclear fusion applications [23]. Under these assumptions, normal operation and unmitigated upward disruption TQ were modelled.

5.1 EU DEMO scenario: normal operation

A 2D stationary simulation under 1.5MW/m^2 was conducted to assess the temperature distribution during normal operation. Computational time was spared by modelling the lattice armor as an homogenized body provided with smeared and anisotropic properties, following the procedure established in [24]. As showed in Figure 6, the maximum temperature of the lattice did not exceed 850°C and that of the heat sink was quite below 390°C, both being compatible with the limits suggested in [25]. We also assessed the heat flux peaking factor, equal to 1.24.

Being the normal operation the initial condition of the transient analysis, the steady state case was solved also on a smaller but more detailed portion of the component where the 3D CAD geometry of the lattice was retrieved and meshed with 650k 10-node-tet elements. In the previous section, we described how the heat load provided by charged particles was implemented. In this section, a similar procedure was followed, considering shallower grazing angles imposed by the tangential B-field lines but also neglecting any temperature dishuniformity on the exposed surface. The input heat flux in ANSYS can be derived from the power balance in stationary conditions:

$$q = q_0 \frac{A_{max}}{A_{eff}}$$

where q_0 is the design heat flux, A_{max} the area available for heat exhaust at the coolant side and A_{eff} the lattice's top surface where the heat flux is applied. The ratio A_{max}/A_{eff} is 2.12 for B samples and 1.48 for A samples.

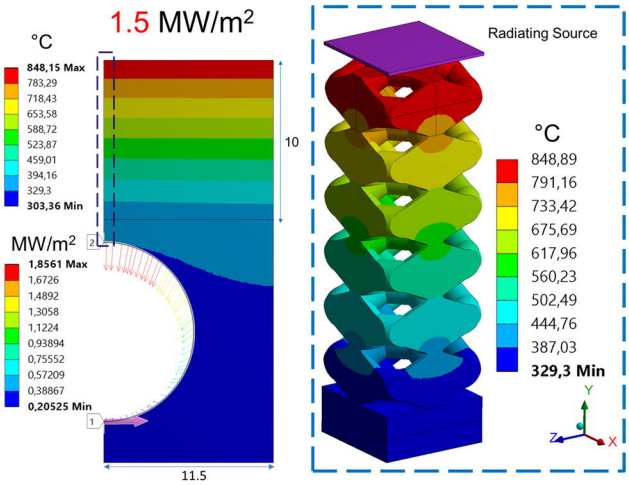

Figure 6: Temperature distribution during normal operation of the UL in the EU DEMO. Both 2D (left side) and 3D (right side) results are in tight agreement. In the 2D analysis, the heat flux legend refers to the vector plot along the cooling pipe. The temperature of the plain source in the 3D analysis, which represents the hot plasma in the 3D analysis, can be calibrated to radiate the load to the lattice

An important feature of our thermal model is that we can not only implement loads from charged particles, but also from radiation or a mixture of both. This is of paramount importance in view of DEMO: as suggested in [6], during flattop particle transport associated to blobs could lead to a broadening of the far scrape-off-layer, with power decay length up to 50mm [26]. In other words, being the UL protruding towards the plasma, it is very likely that a significant fraction of its nominal power will be provided by charged particles during stationary operation.

It is key to remark that the model does not simulate the complex physics of plasma. In the model the amount of heat is an input applied to the complex target geometry. Plasma physics, instead, is taken into account in terms of input power and radiated power fraction, which are key parameters to be determined with dedicated codes (e.g. ASTRA, SOLPS, CHERAB, PFCFlux). In this view, here we put emphasis on the simplified case of totally radiated heat. Radiation from a plane source was assumed as the simplest approach for coupling the desired power with the complex features of the lattice during the normal operation. Plasma was therefore substituted with a plane source radiating at a tunable temperature T_s, whose first estimation can be obtained from the following expression derived from the power balance only between the source and the top surface of the lattice

$$T_s = \left(\frac{q_0}{\sigma F_{s,t}} + T_{max}^4 \right)^{1/4}$$

σ is the Stefan-Boltzmann constant, T_{max} the maximum temperature of the lattice (available from the 2D thermal analysis) and $F_{s,t}$ the view factor, taken from existing analytical solutions valid for parallel and coaxial square surfaces with different dimensions [27]. A more accurate tuning of T_s can be carried out using the ANSYS radiosity solver, which automatically provides the matrix of the view factors between the source and the i-th face of each element of the target, including the inner surfaces of the lattice. In the present work, where 1.5MW/m^2 were set, the corresponding temperature of the source was 2040°C for the A278 lattice and 2055°C for B278. The heat flux peaking was also accounted after the calibration. The resulting temperature distribution is reported in Figure 6, and shows almost perfect agreement with the homogenized case. This analogy suggests also that most of the radiated power (above 80%) is provided to the very top plasma facing surface of the first cell.

5.2 EU DEMO scenario: transient operation

The unmitigated upward disruption TQ was modelled by imposing 5GW/m^2 for 2ms according to [6]. This huge load is expected to be delivered by charged particles impinging the top of the lattice. Non-linear W properties were applied as well as initial conditions imported from the 3D steady state analysis. The transient analysis was carried out in the ANSYS Mechanical APDL environment, where we could implement an original MAPDL routine which removes the mesh elements when they reach a user-defined threshold.

The routine is executed with a defined frequency along the total duration of the transient. Before solving the subsequent timestep, it also reselects the “alive” elements remained at the top and applies accordingly the load. Results are shown in Figure 7, where the threshold was set at the melting temperature, under the hypothesis that the liquid phase is completely removed from the loaded area, e.g. by gravity, splashing or magneto-hydro-dynamic drifts, as observed in existing tokamaks [28]. The component erosion at the end of the transient was found to be near 450 μm in absence of vapour shielding. This value is in the same order of magnitude of existing predictions, e.g. from TOKES [29] and RACLETTE [4] codes, which however are predicted for dense W. The first reference suggests (in absence of vapour shielding) up to 800um of armour erosion at higher energy deposit, while the second one 100um at the same energy. This suggests that the lattice could actually promote the heat flux reduction by means of latent heat and vapour shielding, as its erosion is typically higher than that of dense W.

6. Conclusion

In the present work, we have compared thermal FE analyses and preliminary evidences from the preliminary experiments at the QSPA-Kh50 facility [16], carried out by CCFE on W lattice samples. Non-linear material properties including enthalpy changes of W were implemented to simulate melting and vaporization during fast transients. Model validation in the vaporization regime is still ongoing, but good agreement was suggested by replicationg existing studies and experiments [30]. Similarity with the available data from experiments was confirmed and near perfect agreement up to melting between non-linear W and the ITER SDC-IC reference. Maximum temperatures achieved by lattice samples were found in agreement with the expected incipient melting at 0.6MJ/m^2 and melting occurring under 0.85MJ/m^2 absorbed energy densities. Simulation confirmed also that the pulse duration of 0.25ms is too short for appreciating the different behavior of lattice samples with respect to bulk W. Additional experiments at higher loads and longer pulses will be envisaged, being also more realistic in view of DEMO. These experiments will be also carried on B lattices with polished surfaces, to assess the impact of surface roughness during test and for a proper study of the surface modifications caused by the plasma exposure.

Moreover, ongoing tests at QSPA-Kh50 on polished B samples and will be instrumental for model calibration. Finally, the thermal response of W lattices armors under the normal and transient conditions predicted for the EU DEMO upper limiter was implemented in ANSYS under conservative assumptions.

Steady state simulations under 1.5MW/m^2 were carried out on 2D and 3D geometries and confirmed tight agreement between the two models. The lattice and the heat sink work respectively below 850°C and 390°C, so

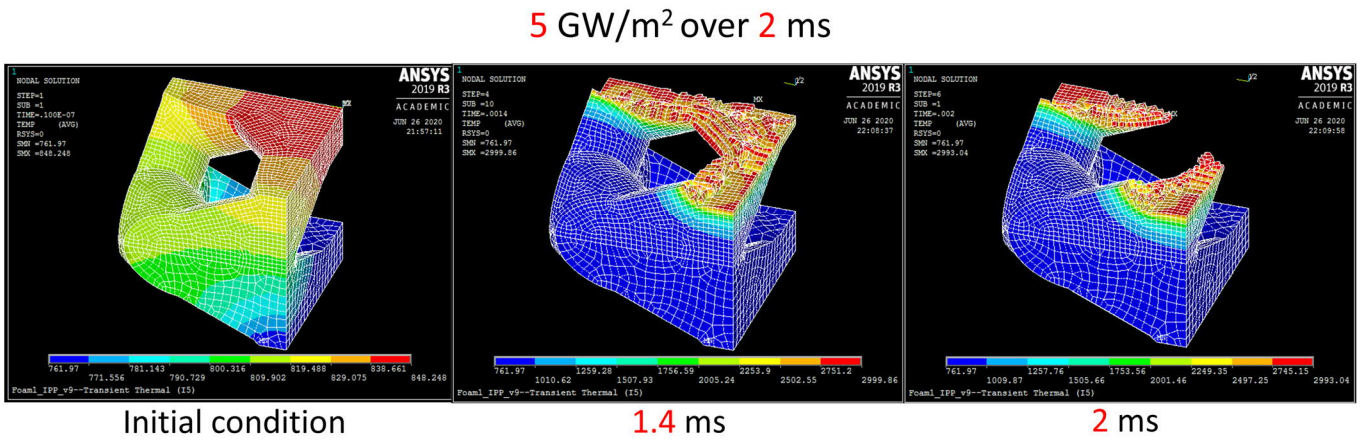

Figure 7: Temperature distribution in the lattice during transient operation. Initial conditions have been imported from the 3D steady state thermal analysis and showed on the left side, indeed the minimum temperature is constant at 762°C, coherently with the applied initial conditions. One can also see the gradients and erosion after 1.4ms and 2ms. A MAPDL routine removes the mesh elements when they reach the melting point and applies again the heat load to the "alive" top elements. Indeed, maximum T of "alive" elements is always around 3000°C in these cases, confirming that the rountine works properly. Total erosion is around 450 µm

within their optimal operating range. In the 3D stationary simulation, radiosity solver was employed in 3D simulation to setup the radiative problem between plasma and the complex geometry lattice. However, the model offers the valuable feature of defining the load in terms of radiation, charged particles' power or a mixture of both. In view of more detailed simulations of the thermal response of the lattice in the upper limiter in DEMO, the proper mix of radiated and conducted load can be applied according to recent predictions [31]. Moreover, the impact of the grazing angle and the gyro motion of charged particles impacting the lattice should be further investigated and, if signicant, it will be included in the stationary simulation.

Steady state 3D results were imposed as initial condition for the following unmitigated disruption TQ modelled as 5GW/m^2 delivered for 2ms by charged particles. An original MAPDL routine which removes the mesh elements when they reach a user-defined threshold (here set at melting) was employed. The lattice erosion during the transient was assessed, with a maximum value in order of 450µm that confirms higher erosion with respect to available predictions for dense W at same energy deposited, as desired in order to promote vapour shielding formation.

Acknowledgements

This work has been carried out within the framework of the EUROfusion Consortium and has received funding from the Euratom research and training program 2014-2018 and 2019-2020 under grant agreement No 633053. The views and opinions expressed herein do not necessarily reflect those of the European Commission.

References

[1] F. A. J. H. Donnè, Philosophical Transactions of the Royal Society A: Mathematical, Physical and Engineering Sciences, vol. 377, no. 2141, p. 20 170 432 (2019).
[2] T. R. Barrett, et al. Fus. Eng Des. 109–111, 917–924, (2016)
[3] A. v. Müller, et al. Nuc. Mat En. 19, 184–188, (2019)
[4] F. Maviglia, et al., Fus. Eng. and Des., Vol. 136, Part A, 410-414 (2018)
[5] E. Nardon, 9th ITER International School, (2017).
[6] R. Wenninger, et al., Nuc. Fus. 57, 046002(11pp) (2017).
[7] E. J. Strait, et al., Nucl. Fusion 59, 112012, (2019).
[8] T. R. Barrett, et al., Nuc. Fus. 59, 056019, (2019).
[9] S. Pestchanyi, et al., Fus. Eng. Des. 109-111, 141-145 (2016).
[10] R. De Luca, et al., Fus. Eng. Des. 158, 111721 (2020).
[11] S. Sharafat, et al., J. Nuc. Mat. 347, 217- 243 109-111 (2005).
[12] M. Andersen, et al. Fus. Eng. Des. 81, 1639–1645 (2006).
[13] A. von Müller, et al., Nuc. Mat. En. 19,184–188, (2019).
[14] P. Fanelli, et al., Mat. Des. 114, 167-175 (2017).
[15] A. von Müller, et al., Mat. Tod. 39, 146-147, (2020).
[16] Mike Fursdon, et al., Final Report EFDA_D_2MNGUC (2020).
[17] P. Tolias, et al., Nuc. Mat. En. 13, 42-57 (2017).
[18] J. W. Arblaster, J. Phase Equilib. Diff., 39, no. 6, 891-907, (2018).
[19] V. A. Makhlai, et al., EHHF discussion, KIPT (2019).
[20] I. E. Garkusha, et al., J. Nuc. Mat. 390–391, 814–817 (2009).
[21] G. Guglielmini, et al., "Elementi di Trasmissione del Calore", CEA Editor, ISBN 9788808083036 (1996)
[22] J. H. You, et al., Nuc. Mat. En. 16, 1–11 (2018) .
[23] E. Rabaglino et al., XVIII Congresso Nazionale sulla Trasmissione del Calore (2000).
[24] R. De Luca, et al., Fus. Eng. Des. 146,1690–1693 (2019).
[25] J. H. You, Nuc. Mat. En. 5, 7-18 (2015)
[26] F. Maviglia, Fus. Eng. Des. 158, 111-713 (2020) .
[27] M. Crawford, paper no. ASME 72-WA/HT-16 (1972).
[28] G. F. Matthews, et al, Phys. Scr. T167, 14-70 (2016).
[29] S. Pestchanyi & F. Maviglia, Fus. Sc. Tech. 75, 647–653 (2019).
[30] A. Cardella, et al, J. Nuc. Mat. 283-287, part 2, 1105-1110 (2000)
[31] F. Maviglia, Nuc. Mat. En. 26, 100897 (2021)